

# Advances in Interferometric Surface Measurement

James C. Wyant

College of Optical Sciences, University of Arizona, Tucson, AZ 85721  
[jcwyant@optics.arizona.edu](mailto:jcwyant@optics.arizona.edu), <http://www.optics.arizona.edu/jcwyant>

## ABSTRACT

The addition of electronics, computers, and software to interferometry has provided tremendous improvements in the measurement of surface shape and roughness. This talk will describe three such improvements; use of computer generated holograms for testing aspheric surfaces, techniques for performing interferometric measurements more accurate than the reference surface, and two single-shot phase-shifting interferometric techniques for reducing the sensitivity of an optical test to vibration and measuring dynamically changing surface shapes.

**Keywords:** Interferometry, optical testing, metrology, phase measurement, measurement

## 1. INTRODUCTION

Improved computers, electronics, and software have helped make possible enormous improvements in the measurement of surface shape and surface roughness. These measurement enhancements have made possible enormous improvements in the fabrication of precision optics, hard disk drives, machine tools, and semiconductors. This talk will discuss three areas where interferometric measurement improvements have been made: 1) The use of computer generated holograms for the testing of aspheric optics, 2) techniques for performing interferometric measurements more accurate than the reference surface, and 3) two single-shot phase-shifting interferometric techniques for reducing the sensitivity of an optical test to vibration and measuring dynamically changing surface shapes.

## 2. COMPUTER GENERATED HOLOGRAMS (CGH)

It has been more than 36 years since Lohmann and Paris first described computer generated holograms (CGHs)<sup>1</sup> and CGHs have been used to test aspheric optical elements for more than 35 years<sup>2</sup>. Computer generated holograms are now widely used in the testing of aspheric optical elements and it is expected that their use in aspheric testing will greatly increase the next few years as the superb measurement capability of CGHs are better appreciated by more optical manufacturing personnel. While CGHs are most often used to test rotationally symmetric surfaces, a great advantage of CGHs is that they can be made for testing free form optics almost as simply as for testing rotationally symmetric optics. Crosshairs can be put on the CGH to aid in the alignment of the CGH and additional holograms can be placed on the CGH to aid in the alignment of the optics or to aid in calibration of the CGH. CGH interferometers work well with phase-shifting techniques. Figure 1 shows one setup for using a CGH to perform an optical test and Figure 2 shows a typical CGH.

The CGH can be thought of as a binary representation of the interferogram, or hologram that would be recorded if we were to interfere the aspheric wavefront coming from a perfect aspheric surface with the reference beam. The procedure for making the CGH is to first raytrace the interferometer to determine the position of the fringes in the theoretical interferogram that would be obtained if the mirror under test were perfect. A plotter, such as a laser beam recorder or an e-beam recorder, is then used to draw lines along the calculated fringe positions.

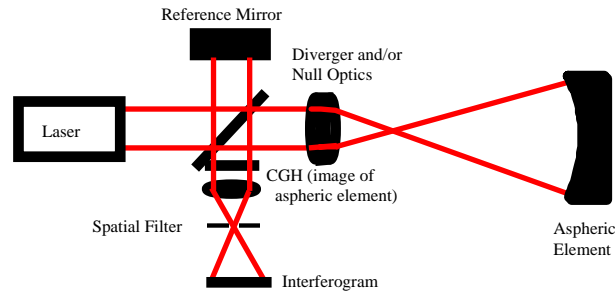


Figure 1. Typical CGH Interferometric Setup.

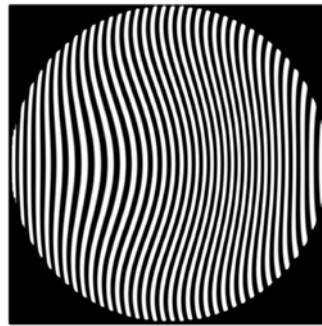


Figure 2. Typical CGH.

When the CGH is placed in the interferometer as shown in Fig. 1, the CGH and the interference fringes produced by the interference of the reference wavefront and the wavefront produced by the mirror under test produce a moiré pattern that gives the difference between the CGH and the interference fringes. If sufficient tilt is introduced into the CGH to separate the diffraction orders of interest, spatial filtering can be used to improve the contrast of the moiré pattern. Spatial filtering is accomplished by reimaging the hologram with an appropriately placed small aperture in the focal plane of the reimaging lens. This aperture is placed such that it passes only the wavefront from the mirror under test and the +1 order beam resulting from illuminating the hologram with a plane wavefront, or equivalently passing the reference beam and the -1 order produced by illuminating the hologram with the aspheric wavefront. In the first case we are interfering two aspheric wavefronts, one produced by the aspheric mirror and the second produced by the CGH. In the second case we are interfering two plane waves, one produced by the reference arm and the second produced by the CGH removing the asphericity in the test beam. The requirement for being able to accomplish this spatial filtering is that in the making of the CGH, the slope (tilt) of the plane reference wavefront is at least as large as the maximum slope of the aspheric wavefront along the intersection of the plane of incidence of the plane wave and the aspheric wavefront. Thus, in the interference plane shown, an interferogram is produced that gives the difference between the wavefront produced by the mirror under test and the corresponding wavefront produced by the hologram.

There are many places in the interferometer where a CGH could be placed. One reason it is placed as shown is that thickness variations in the hologram plate have no effect on the results, and thus what could be a very serious source of error is eliminated. A second reason is that the CGH is used in single pass so its diffraction efficiency need not be high. It should be stressed that the above raytracing procedure used to make the holograms can be used for any general optical system. The only requirement is that all the optics in the interferometer be known so the system can be raytraced. An important consequence of raytracing the entire interferometer is that even though the diverger may be corrected only for spherical wavefronts and may introduce additional aberrations in the aspheric wavefront being passed through it, the hologram automatically corrects for these aberrations when a null test (or for all practical purposes, a near null test) is performed.

Figure 3 shows a more common arrangement for placing the CGH in the interferometric setup. An advantage of this setup is that it can be used with commercial interferometers without any need for modifying the interferometer. A

second very large advantage is that since the CGH is placed between the asphere and the diverger lens it is not necessary to include the diverger lens in the raytrace and hence it is not necessary to precisely know the design of the specific diverger lens being used. However, in this setup the quality of the CGH substrate must be known so errors introduced by it can be subtracted from the test results.

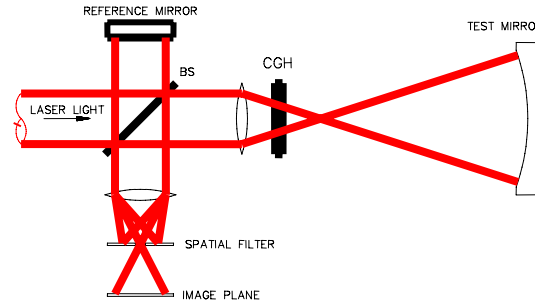


Figure 3. Common setup for using a CGH as a null lens.

The largest source of error is in the drawing of the grating lines<sup>3,4</sup>. To show how the CGH wavefront accuracy depends upon the number of distortion free plotter resolution points and the maximum slope of the aspheric wavefront being tested, let us suppose the plotter has  $P \times P$  resolution points. Thus, there are  $P/2$  resolution points across the radius of the hologram. Since by definition the maximum error in plotting any point is one-half of a resolution unit, any portion of each line making up the hologram could be displaced from where it should be a distance equal to  $1/P$  the radius of the hologram. Let the maximum difference between the slope of the aspheric wavefront and the tilted plane wave be  $S$  waves per hologram radius. Thus, the phase of the plane wave at the hologram lines can differ from that of the required wavefront at the same lines by as much as

$$2\pi(S/P) \text{ radians or } S/P \text{ waves}$$

Therefore, in the hologram plane the error in the reconstructed wavefront can be as large as  $S/P$  waves. In other words, the accuracy is determined by the accuracy with which we draw the grating lines. If we have an error in drawing a grating line of  $1/100$  the grating spacing, then the resulting error is  $1/100$  wave.

Figure 4 shows a plot of the OPD and slope of an aspheric wavefront. For this example the maximum OPD is approximately 300 waves (fringes) and the maximum slope is 500 waves/radius. If in the hologram we introduced enough tilt fringes to separate the first and second orders the maximum slope being measured would be 4 times this, or 2000 waves/radius<sup>3</sup>. If we used a plotter having a distortion free resolution cell size of 0.5 microns and a hologram diameter of 50 mm we would have  $10^5$  resolution points and the maximum error resulting from the hologram plotter would be  $1/50$  wave.

Plotter errors can be measured and removed in the data reduction if either orthogonal straight line gratings or circular zones plates are drawn on the CGH along with the grating used to produce the aspheric wavefront. The straight line gratings will produce plane waves which can be interfered with a reference plane wave to determine plotter errors<sup>5, 8</sup>. The circular zone plates will produce a spherical wave which can be interfered with a reference spherical wave to again determine plotter errors.

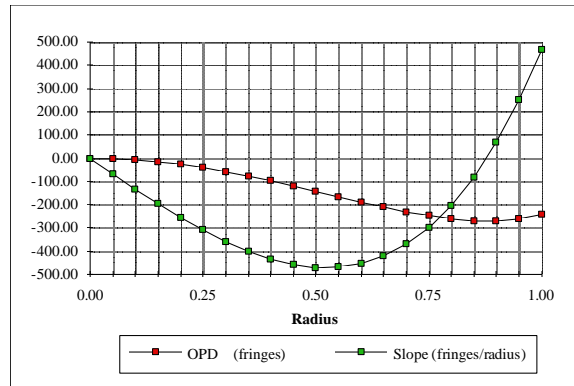


Figure 4. Wavefront departure and slope versus radius.

Errors can also result from the hologram being in the wrong location. Errors due to a longitudinal misalignment are less critical in the setup shown in Figure 1 than for Figure 2 because the hologram is placed in nearly collimated light. Lateral displacement errors give errors proportional to the derivative (i.e. slope) of the wavefront<sup>3</sup>. Generally alignment marks, crosshairs, are placed on the CGH to aid in the alignment.

Another good feature of a CGH test is that additional holographic structures can be placed on the CGH to produce alignment spots for the optical setup shown in Figure 1 or 3 to aid in the alignment of the optical system under test. Figure 5 shows fiducial marks produced by a CGH. The positions of the crosshairs can be controlled to micron accuracy.

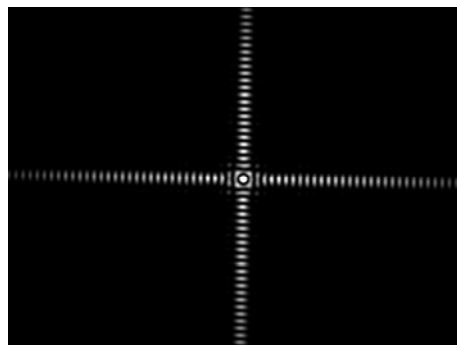


Figure 5. Fiducial marks produced by a CGH 15 meters from the CGH. The central lobe is 100 microns FWHM.

### 3. PERFORMING INTERFEROMETRIC MEASUREMENTS MORE ACCURATE THAN THE REFERENCE SURFACE

There are several techniques for performing measurements of flat surfaces, spherical surfaces, or surface roughness that are more accurate than the reference surface<sup>9, 10</sup>. All of these techniques require making multiple measurements while rotating or translating the surface under test and performing arithmetic calculations on the measured data. While these techniques have been available for many years, it is only due to the high precision of phase-shifting interferometry (PSI) that the techniques have become extremely useful for improving the ability to produce high quality optical surfaces.

#### 3.1 Absolute measurement of flat surfaces

Absolute measurements of flat surfaces are also available, although the most popular technique gives only profiles through the surface<sup>11</sup>. To obtain x and y profiles from an absolute measurement of a flat surface, four measurements and three flats are required. Figure 6 shows the four measurements required of flats A, B, and C.

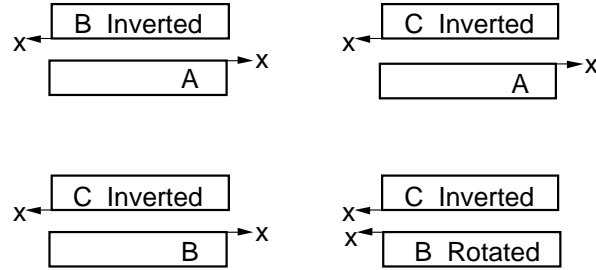


Figure 6. Four measurements required for three-flat test.

If  $G(x,y)$  is a measurement, and  $f(x,y)$  is the surface error of a flat, the four measurements give

$$G_{AB}(x,y) = f_A(x,y) + f_B(-x,y)$$

$$G_{AC}(x,y) = f_A(x,y) + f_C(-x,y)$$

$$G_{BC}(x,y) = f_B(x,y) + f_C(-x,y)$$

$$G_{BC'}(x,y) = f_B(-x,-y) + f_C(-x,y)$$

From these four equations it is possible to solve for both the x and y profile of the three flats. For example, the x profile of the three flats is given by

$$f_A(x,0) = \frac{G_{AB}(x,0) + G_{AC}(x,0) - G_{BC'}(x,0)}{2}$$

$$f_B(x,0) = \frac{G_{AB}(x,0) - G_{AC}(x,0) + G_{BC'}(x,0)}{2}$$

$$f_C(x,0) = \frac{-G_{AB}(x,0) + G_{AC}(x,0) + G_{BC'}(x,0)}{2}$$

Once the x profile is known for the reference flat, the reference flat can be used to find additional profiles for a test flat.

### 3.2 Absolute measurement of spherical surfaces

Computer techniques make it possible to subtract interferometer errors from errors in a spherical mirror being tested if three measurements are performed<sup>12</sup>. Figure 7 shows the three measurements required. First the mirror is tested at center of curvature using common techniques. Next the mirror is rotated 180 degrees and the measurement is repeated. The third measurement is performed by placing either a flat mirror or the mirror under test at the focus of the diverger lens. If  $W_{ref}$  is the error due to the reference arm of the interferometer,  $W_{div}$  is the error due to the diverger lens, and  $W_{surf}$  is the error due to the spherical mirror under test, the three measurements give

$$W_{0^\circ} = W_{\text{surf}} + W_{\text{ref}} + W_{\text{div}}$$

$$W_{180^\circ} = \overline{W}_{\text{surf}} + W_{\text{ref}} + W_{\text{div}}$$

$$W_{\text{focus}} = W_{\text{ref}} + \frac{1}{2} [W_{\text{div}} + \overline{W}_{\text{div}}]$$

The bar over the symbol means the quantity has been rotated 180 degrees. The error due to only the mirror surface is obtained by combining these three measurements.

$$W_{\text{surf}} = \frac{1}{2} [W_{0^\circ} + \overline{W}_{180^\circ} - W_{\text{focus}} - \overline{W}_{\text{focus}}]$$

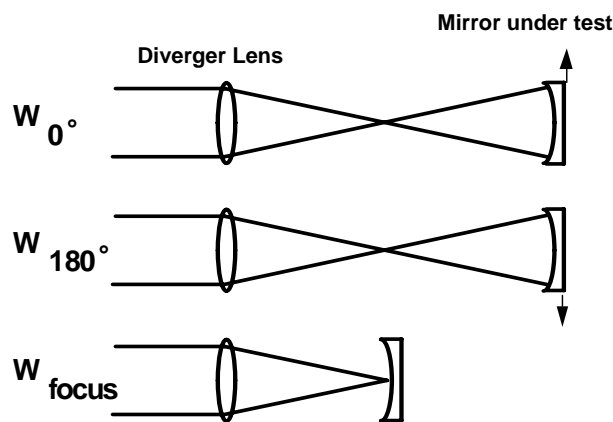


Figure 7. Three measurements required for absolute spherical mirror testing.

Figure 8 shows typical results for removing interferometer errors from the measurement of a spherical mirror.

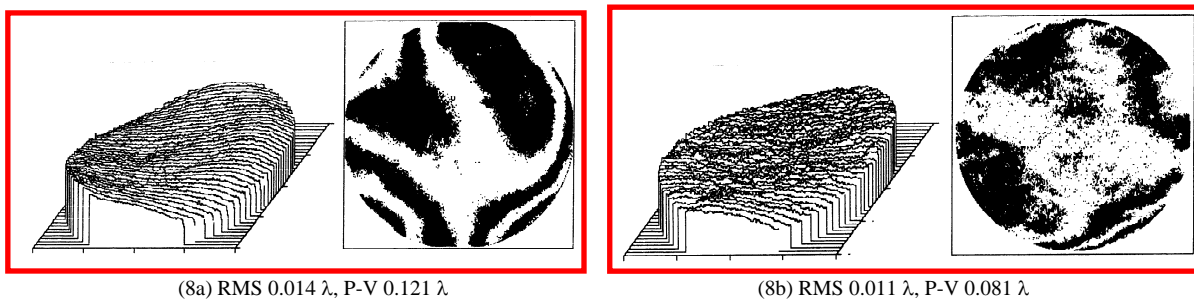


Figure 8. (a) Measurement of spherical mirror with interferometer aberrations, (b) Measurement of spherical mirror after interferometer errors are removed.

### 3.3 Absolute measurement of surface roughness

Due to powerful computer techniques it is possible to interferometrically measure surfaces smoother than the reference surface in the interferometer. As described below, errors in the reference surface can be removed enabling a person to routinely measure sub-Angstrom surface microstructure, even with a much rougher reference surface<sup>13</sup>.

Each measurement made with an interferometric optical profiler yields the relative point-by-point distance between the reference and test surfaces. Assuming the test and reference surfaces are uncorrelated and independent of one another, the rms roughness  $\sigma_{\text{meas}}$  of the interferometric measurement is a combination of the two rms roughness values:

$$\sigma_{\text{meas}} = \sqrt{\sigma_{\text{test}}^2 + \sigma_{\text{ref}}^2},$$

where  $\sigma_{\text{test}}$  is the rms roughness of the surface under test and  $\sigma_{\text{ref}}$  is the rms roughness of the interferometer reference surface.

To subtract the effects of the reference surface in the interferometer, three different techniques can be implemented. A straightforward means of producing a reference surface profile is to measure a supersmooth mirror with an rms roughness of less than 1 Å. This information can be stored in the computer and subtracted from each measurement.

Another technique is to create a profile of the reference surface by averaging a number of measurements,  $N$ , of a smooth mirror. The mirror surface used to do the averaging does not need to be supersmooth, but the smoother it is, the fewer measurements will need to be averaged. Between measurements, the mirror is moved by a distance greater than the correlation length of the surface. The roughness of the mirror being measured tends to cancel out and the result obtained after averaging approximates the reference surface. The resulting rms roughness measurement error is given by

$$\sigma_{\text{error}} = \frac{\sigma_{\text{mirror}}}{\sqrt{N}},$$

where  $\sigma_{\text{mirror}}$  refers to the rms roughness of the mirror surface used to produce the generated reference profile. Thus, the error in the measurement of the test surface rms roughness is reduced by using a smoother mirror to generate the reference and by increasing the number of measurements averaged to generate the reference. Once the reference surface profile is generated, it can then be subtracted from subsequent measurements of test surfaces to measure the surface profile minus the reference surface. Using this procedure, supersmooth surfaces with rms roughness values of less than an Ångstrom can be measured.

A simple technique for obtaining the rms roughness of a supersmooth surface, but not the profile, is to use the so called absolute rms roughness measurement technique. For the absolute rms roughness measurement, two uncorrelated measurements of the test surface are made. To get an uncorrelated measurement, the test surface is moved between measurements a distance greater than the correlation length of the surface. Since the reference surface effect on the measured profile should not change from the first to the second measurement, the effects of the reference surface profile cancel out when the difference of these two measurements is taken. If we assume the two measurements,  $\text{test}_1$  and  $\text{test}_2$ , are uncorrelated, the rms roughness of the difference profile can be written as

$$\sigma_{\text{diff}}^2 = \sigma_{\text{test}_1}^2 + \sigma_{\text{test}_2}^2.$$

Because independent measurements of the test surface profile should have similar statistics,

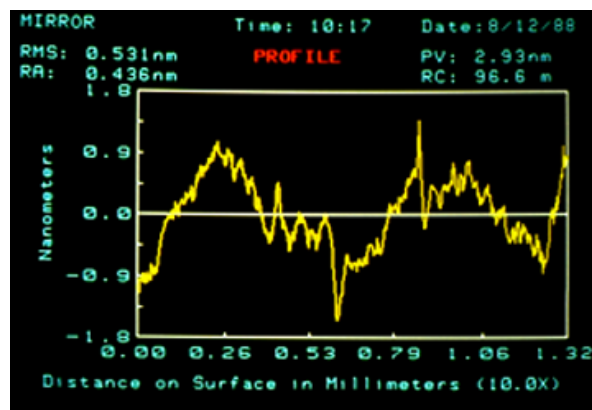
$$\sigma_{\text{test}_1} = \sigma_{\text{test}_2}.$$

The rms roughness of the test surface is given by

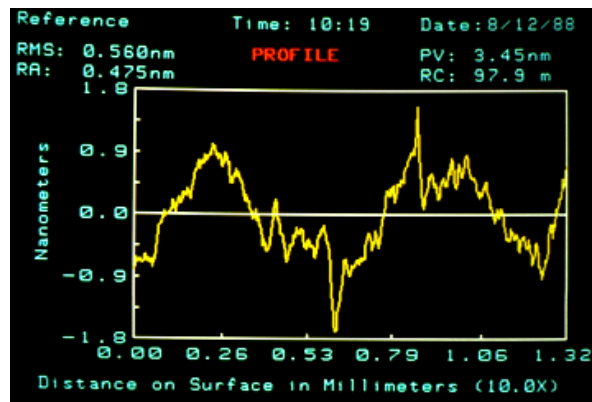
$$\sigma_{\text{test}} = \frac{\sigma_{\text{diff}}}{\sqrt{2}}$$

Thus, the rms roughness of the test surface can be easily determined by making two measurements of the surface. When this measurement is made, the effects of the reference surface cancel, and the surface statistics are derived. However, the calculated surface profile does not represent the actual test surface.

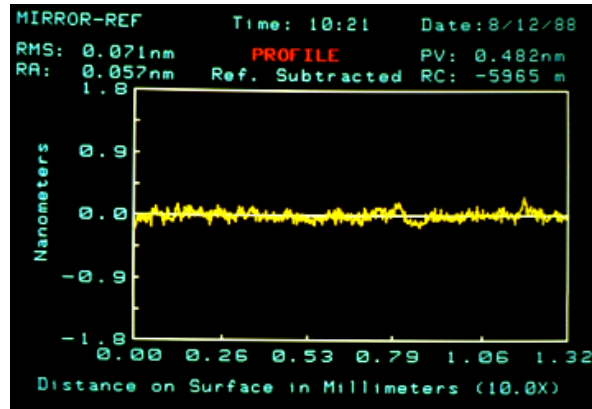
Figure 9 shows measurement results for a supersmooth mirror. Figure 9a shows the profile of the supersmooth mirror with the effects of errors in the reference surface remaining. Figure 9b shows the profile of the reference surface obtained by averaging sixteen uncorrelated measurements of the supersmooth mirror. Figure 9c shows the profile of the supersmooth surface obtained by subtracting the profile shown in Figure 9b from the profile shown in Figure 9a. Note that the vertical scale for Figure 9c is different from that of Figures 9a and 9b. The supersmooth mirror is found to have an rms surface error of 0.71 nm. Measurements performed using the absolute rms technique gave a similar result of 0.70 nm.



(a)



(b)



(c)

Figure 9. (a) Profile of a supersmooth mirror including effects of reference surface. (b) Profile of reference surface. (c) Difference between 4a and 4b showing the profile of the supersmooth mirror without the effects of the reference mirror.

The use of a computer with an optical testing interferometer creates a much more powerful system than the interferometer by itself. Being able to perform optical tests more accurate than the reference can go a long way in improving the quality of optical systems produced.

#### 4. VIBRATION INSENSITIVE INTERFEROMETERS

The measurement accuracy of phase-shifting interferometry (PSI) is generally limited by the environment. In PSI it is important to change the phase difference between the two interfering beams between intensity measurements in a controlled manner. This is where the environment becomes critical, because vibration or air turbulence can change the phase difference between the two beams in unknown ways and hence introduce large errors in the measurement. Techniques such as carrier frequency interferometry, closed-loop feedback vibration compensated interferometry, and single-shot phase-shifting interferometry can be used to reduce the effect of the environment.

A superior approach is to have all four phase-shifted frames fall on a single CCD camera as shown in Figure. 10. In this arrangement, an interferometer is used where a polarization beamsplitter causes the reference and test beams to have orthogonal polarization. After the two orthogonally polarized beams are combined they pass through a holographic element that splits the beam into four separate beams resulting in four interferograms. These four beams pass through a birefringent mask that is placed just in front of a CCD camera. The four segments of the birefringent mask introduce phase shifts between the test and reference beams of 0, 90, 180, and 270 degrees. A polarizer with its transmission axis at 45 degrees to the direction of the polarization of the test and reference beams is placed after the phase masks just before the CCD array. Thus, all four phase-shifted interferograms are detected in a single shot on a single detector array<sup>14, 15</sup>.

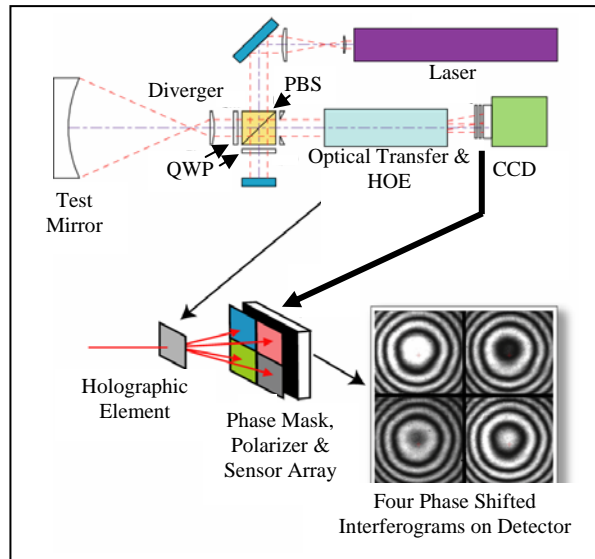


Figure 10. Single shot interferometer (PhaseCam).

By making short exposures the vibration, as well as the air turbulence is frozen. The effects of air turbulence can be reduced by taking many sets of data, where the time between the different data sets is long compared to the time it takes for the turbulence to change, and then averaging the data.

Not only can the effects of vibration be eliminated, but by making short exposures to freeze the vibration the vibrational modes can be measured. Movies can be made showing the vibration. Likewise, flow fields can be measured.

A second approach for dynamic interferometry that will be discussed in this paper is spatial carrier interferometry. In spatial carrier interferometry a single interferogram is taken that has a lot of tilt fringes<sup>16</sup>. The exposure time for the interferogram is short enough that the vibration is frozen. One analysis approach that works with a single interferogram having many tilt fringes present assumes that across a relatively small window the wavefront may be considered flat<sup>17</sup>. Then across the small window the phase varies linearly and the phase difference between adjacent pixels is constant and the normal phase-shifting algorithms can be used. For example, let's assume the tilt between the two interfering beams is selected so there are four detector elements between fringes. In this case the phase of the tilted reference wave changes 90 degrees between adjacent detector elements (360 degrees between fringes). Phase-shifting algorithms can then be used to calculate the phase using the intensities measured by four adjacent detectors. This technique would work well if the test wavefront has no aberrations because then the fringes would be equally spaced. If aberrations are present the fringe spacing changes and the detector spacing is no longer exactly one-quarter the fringe spacing. However, as the aberrations become larger this measurement technique still often works sufficiently well. Many different algorithms have been derived to reduce the requirements on the flatness of the wavefront across the sampling window<sup>18</sup>.

A critical item is the method for obtaining the carrier fringes. An excellent approach that does not require the test and reference beam to have a large angle between them in the interferometer is to have the reference and test beams have orthogonal polarization and then a phase filter is placed directly in front of the detector to introduce a phase difference between the two beams. A phase filter that works especially well because the phase shift between the two interfering beams is nearly independent of wavelength is a quarter waveplate followed by linear polarizers at different angles. The quarter waveplate is oriented to convert the test beam into right-handed circular polarization and the reference beam into left-handed circular polarization. If these circularly polarized beams are transmitted through a linear polarizer a phase shift between the two interfering beams proportional to twice the rotation angle of the polarizer results. Thus, if a phase mask is made of an array of 4 linear polarizer elements having their transmission axes at 0, 45, 90, and 135 degrees as shown in Figure 11, where a polarizer element is placed over each detector element, the mask will produce an array of four 0, 90, 180, and 270 degrees phase shifted interferograms. While an achromatic quarter waveplate could be used to extend the spectral range the phase mask would work for, it turns out that the phase shift produced by the rotated polarizers does not depend greatly upon the quarter-wave plate being a true quarter-waveplate<sup>19</sup>.

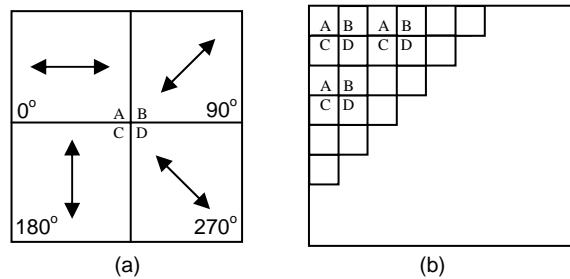


Fig. 11 Phase filter. (a) 4 polarizer elements giving 0, 90, 180, and 270 degree phase shifts. (b) Phase filter made up of array of 4 polarizer elements.

## 5. CONCLUSIONS

The addition of electronics, computers, and software to interferometry has indeed help make tremendous improvements in the measurement of surface shape and roughness. It is expected that these improvements will continue for many years.

## 6. REFERENCES

1. A. W. Lohmann and D. P. Paris, *Appl. Opt.* 6, 1739 (1967).
2. A. J. MacGovern and J. C. Wyant, *Appl. Opt.* 10, 619, (1971).
3. J. C. Wyant and V. P. Bennett, *Appl. Opt.* 11, 2833, (1972).
4. Yu-Chun Chang and James H. Burge, *SPIE Proc.* Vol. 3782, 358, (1999).
5. J. C. Wyant and P. K. O'Neill, *Appl. Opt.* 13, 2762, (1974).
6. Mathias Beyerlein, Norbert Lindlein, and Johannes Schwider, *Appl. Opt.* 41, 2440, (2002).
7. Stephan Reichelt, Christof Pruss, and Hans J. Tiziani, *Appl. Opt.* 42, 4468, (2003).
8. Steven M. Arnold and Robert Kestner, *Proc. SPIE* 2536, 117, (1995).
9. James C. Wyant, *Photonics Spectra*, 97-101, (March, 1991).
10. J. C. Wyant and K. Creath, *Proc. 15th Congress of the ICO*, 568-569 (1990).
11. G. Schulz and J. Schwider, in *Progress in Optics*, Vol. 13, E. Wolf, Ed., North-Holland, Amsterdam, 1976, Chapter IV.
12. A. E. Jensen, "Absolute calibration method for laser Twyman-Green wavefront testing," *J. Opt. Soc. Am.*, **63**, 1313 (1973).
13. K. Creath and J.C. Wyant, "Absolute measurement of surface roughness," *Appl. Opt.* **29**, 3823-3827 (1990).
14. James E. Millerd and Neal J. Brock, "Methods and apparatus for splitting, imaging, and measuring wavefronts in interferometry," U. S. Patent 6,304,330 (2001).
15. James C. Wyant, *Optics & Photonics News*, 14, 4, 36-41 (2003).
16. M. Takeda, "Temporal versus spatial carrier techniques for heterodyne interferometry," in Proceedings, 14<sup>th</sup> congress of the international commission of optics: August 24-28, 1987, Henri Arsenault, ed., *Proc. SPIE* 813, 329-330 (1987).
17. D. M. Shough, O. Y. Kwon, and D. F. Leary, "High speed interferometric measurement of aerodynamic phenomena," in Propagation of high-energy laser beams through the earth's atmosphere, Peter B. Ulrich and Leroy E. Wilson, ed., *Proc. SPIE*, 1221, 394-403 (1990).
18. M. Küchel, "Methods and apparatus for phase evaluation of pattern images used in optical measurement," U.S. Patent 5,361,312 (1994).
19. S. Suja Helen, M.P. Kothiyal, and R.S. Sirohi, "Achromatic phase-shifting by a rotating polarizer", *Opt. Comm.* **154**, 249 (1998).